Electronic Supplementary Material (ESI) for Dalton Transactions.
This journal is © The Royal Society of Chemistry 2023

Supplementary Information

Quaternary heterojunction nanoflower for significantly enhanced electrochemical water splitting

Hao Chen [a], Wanqiu Liu [b], Jiangning Li [a], Wenna Zhao [c,*], Linli Chen [a], Guochang Li [a],Kai Tao [a], Lei Han [a,*]

[a] School of Materials Science & Chemical Engineering, Ningbo University, Ningbo, Zhejiang 315211, China

[b] School of Letters and Science, UC Davis, Davis, California, 95616, United States

[c] School of Biological and Chemical Engineering, Ningbotech University, Ningbo, Zhejiang 315100, China

* Corresponding Author.

E-mail addresses: hanlei@nbu.edu.cn (L. Han); wnzhao@nit.zju.edu.cn (W. Zhao)

Materials

All chemicals were of analytical grade and were used directly without any further purification. Ferric nitrate nonahydrate ($Fe(NO_3)_3·9H_2O$), L-cysteine, nickel nitrate hexahydrate ($Ni(NO_3)_2·6H_2O$), Urea, Potassium hydroxide (KOH), hydrochloric acid (HCl), anhydrous ethanol and acetone were purchased from Sinopharm Chemical Reagent Co. Chemical Reagent Co., Ltd (Shanghai, China). Iridium powder (IrO_2) and platinum carbon powder (Pt/C, 20 wt%) were commercial products from Macklin (China). Naphthofen solution (5 wt%) was purchased from DuPont China Holdings Limited (Tianjin. China). NF with a thickness of 1.5 mm was purchased from Lizhiyuan Ltd. (Shanxi. China). Deionized water was used throughout the experiments.

Nickel foam was treated with hydrochloric acid by sonication for 15 min, followed washed by deionized water and acetone, respectively.

Characterization

The crystalline structure of the sample was characterized by using X-ray diffractometer (Bruker AXS D8 Advance) at 40 kV and 40 mA for monochromatized. Fourier transform infrared (FTIR) spectra were measured using a NICOLET-5700 FTIR spectrophotometer. Inductively coupled plasma-mass spectrometry (ICPMS) were measured using Agilent 7800. Raman spectra were measured using DXR3. Raman Microscope (Thermo Fisher Scientific, USA) at 532nm Laser wavelength. The compositions and micro-structures of the samples were further analyzed by field emission scanning electron microscopy (FESEM, Hitachi S-4800) and transmission electron microscopy (TEM, FEI Talos F200x) equipped with an energy dispersive X-ray spectrometer (EDS). An X-ray photoelectron spectrometer (Thermo fisher Scientific, USA) was used for this experiment. Among them, the working vacuum of the analytical chamber: ~2×10^{-7} mba; X-ray source: monochromatized Al Kα source (Mono Al Kα); energy: 1486.6eV, 6mA×12KV (72W); beam spot size: 30-400μm; Scanning mode: CAE (fixed analyzer energy) full-spectrum scanning; full-spectrum scanning: fluence energy of 100 eV, step size of 1 eV; narrow-spectrum scanning: fluence energy of 30 eV, step size of 0.1 eV; Binding energy correction: surface contamination C1s (284.8 eV) was used as the standard for correction.

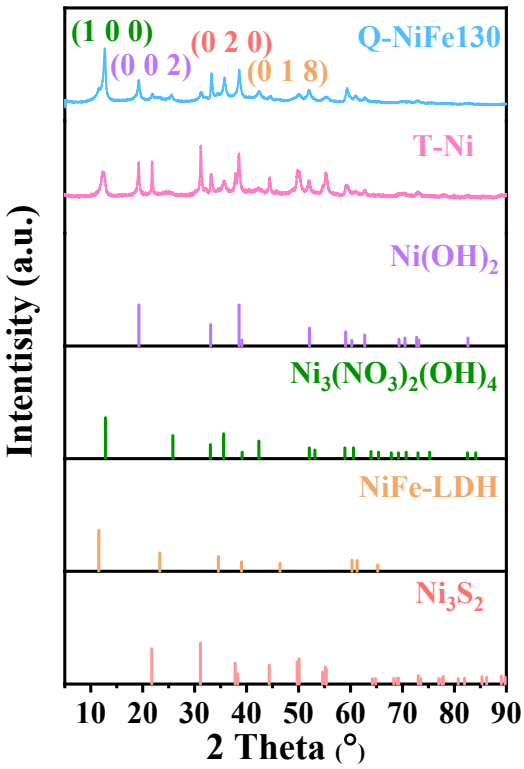

Figure S1. XRD plots of Q-NiFe130 and T-Ni.

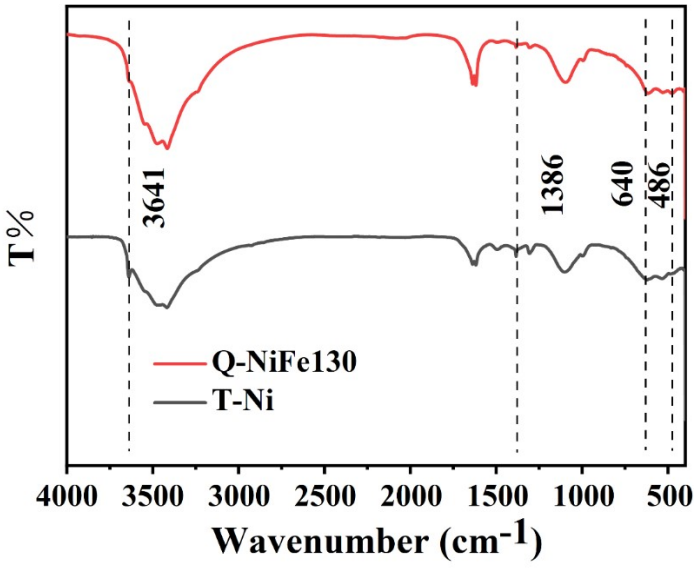

Figure S2. FT-IR spectra of Q-NiFe130 and T-Ni coating.

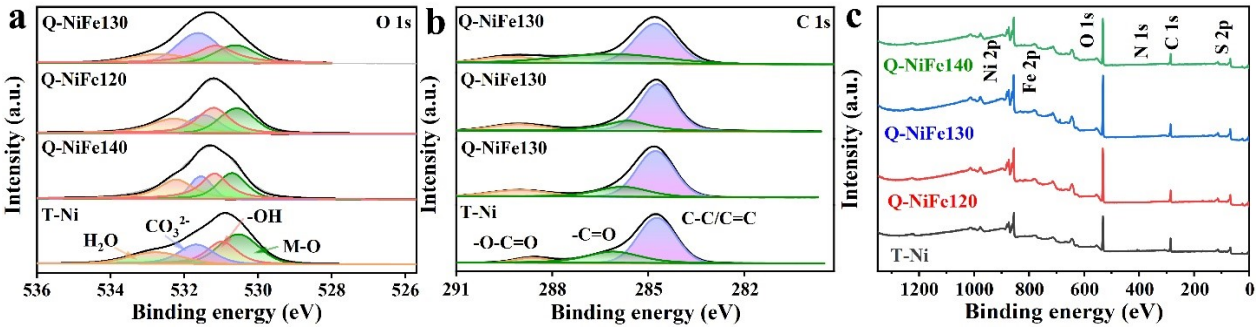

Figure S3. XPS spectra plots of T-Ni, Q-NiFe120, Q-NiFe130 and Q-NiFe140. (a) O1s; (b) C1s; (c) XPS survey spectra plots.

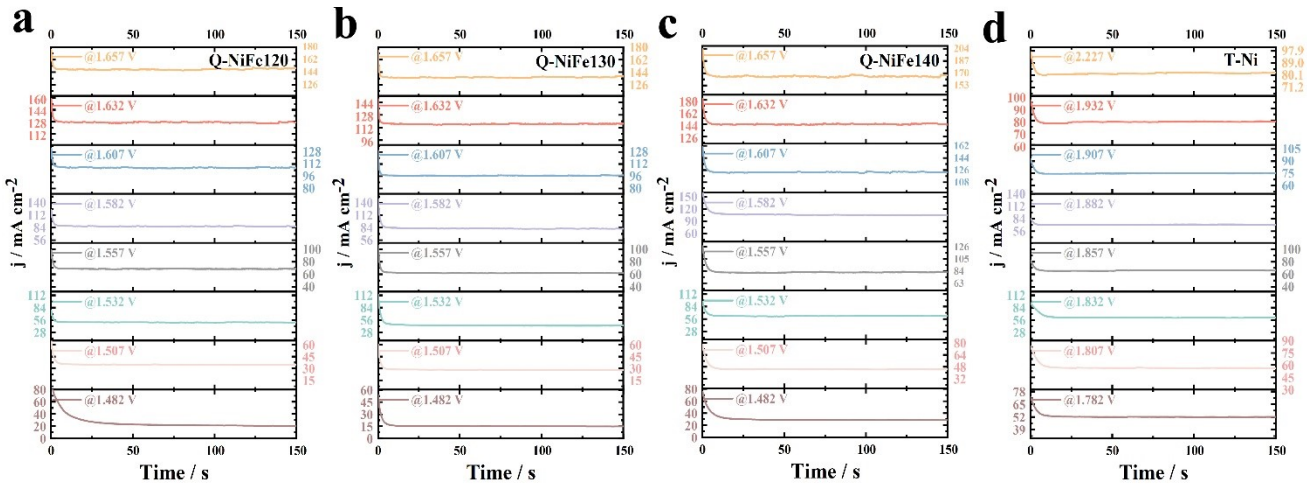

Figure S4. CA responses of activity stabilized T-Ni, Q-NiFe120, Q-NiFe130 and Q-NiFe140 in 1.0 M KOH in the catalytic turnover region.

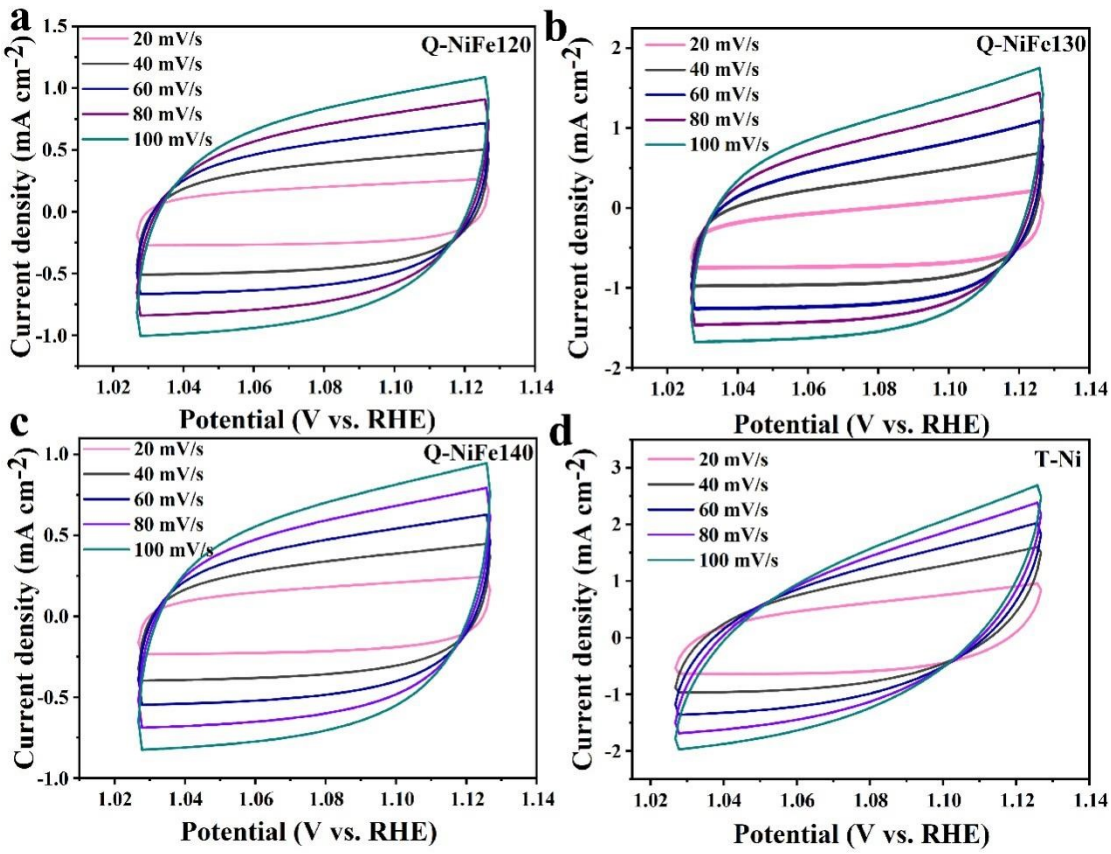

Figure S5. CV curves at different scan rates. (a) Q-NiFe120; (b) Q-NiFe130; (c) Q-NiFe140; (d) T-Ni.

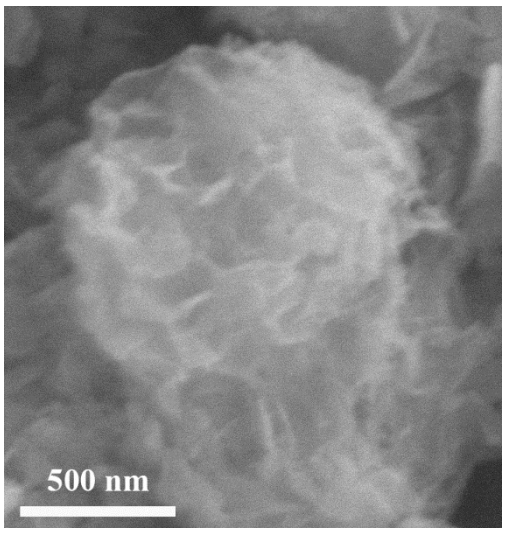

Figure S6. SEM image of Q-NiFe130 after OER reaction for100 h.

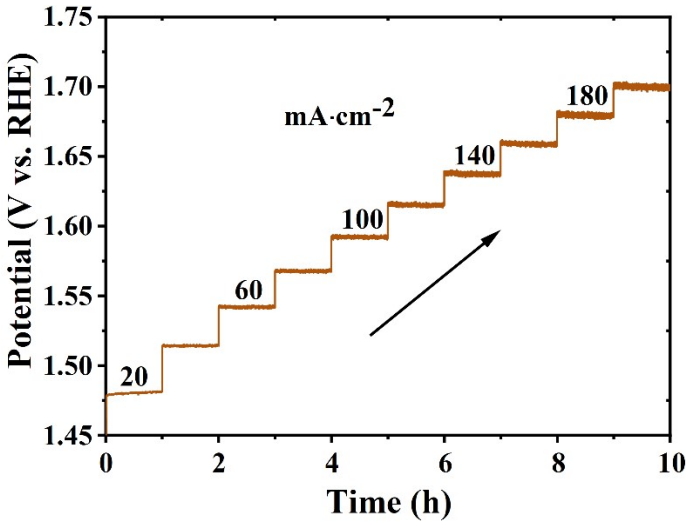

Figure S7. Multistep CP curves with the increment of 20 mA cm^{-2} per 1h in the current range of 20-200 mA cm^{-2}.

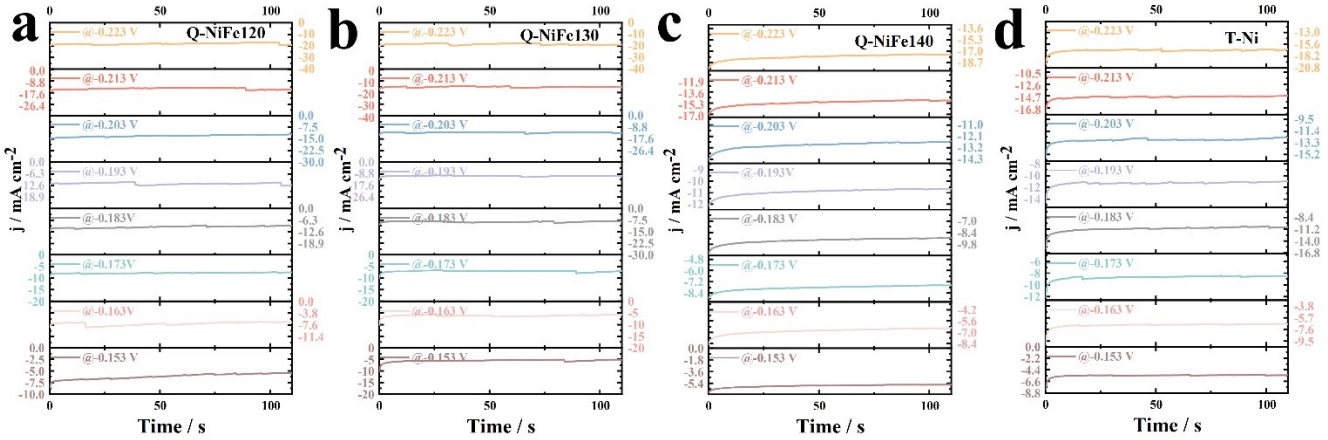

Figure S8. CA responses of activity stabilized T-Ni, Q-NiFe120, Q-NiFe130 and Q-NiFe140 in 1.0 M KOH in the catalytic turnover region.

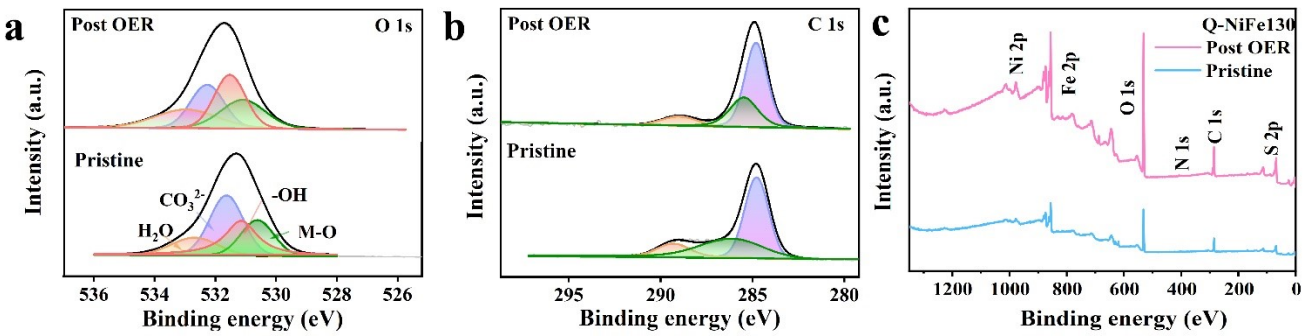

Figure S8. XPS spectra plots of Q-NiFe130 Post OER and Q-NiFe130. (a) O1s; (b) C1s; (c) XPS survey spectra plots.

Table S1. Comparison of OER performances between Q-NiFe130 and other reported electrocatalysts.

Electrocatalysts	**Electroiyte (KOH)**	**j mA/cm^2**	**η （mV）**	**Tafel slope (mV/dec)**	**Ref.**
Q-NiFe130	1M	100	227	60.6	This work
NiSe@NiFe-LDH	1M	100	232	58.2	1
NiFe-LDH $Sn_{0.015(M)}$	1M	10	250	143	2
NiFe-LDH nanoclusters	1M	100	283	56.47	3
CeO_2@NiFe-LDH	1M	10	246	65	4
NiFeCe-LDH/Cp	1M	100	267	31.69	5
NiFe-LDH@$Ni_xCo_ySe_2$/NF	1M	100	265	57.5	6
NiMoP@NiFe-LDH	1M	150	299	23.3	7
$NiCo_2O_4$@NiFe-LDH	1M	50	270	74	8
NFO/3DGN-10	1M	10	272	64	9
NiFe-LDH/Ni/NM	1M	100	236		10

Table S2. ICPMS test results of S

Simple Number	Simple Volume V_0（mL)	Constant Volume V_1（mL)	Test Element	Test Solution Element Concentration C_o（ug/L)	Dilution Ration f	Primary Solution Element Concentration C_1（mg/L)
1	10	10	S	318.284	10	3.183
1	10	10	S	318.554	10	3.186

References

[1] W. Bao, C. Yang, T. Ai, J. Zhang, L. Zhou, Y. li, X. Wei, X. Zou, Y. Wang, Modulating interfacial charge distribution of NiSe nanoarrays with NiFe-LDH nanosheets for boosting oxygen evolution reaction, *Fuel*. 2023, **332**, 126227.

[2] K. Bera, R. Madhu, H.N. Dhandapani, S. Nagappan, A. De, S. Kundu, Accelerating the Electrocatalytic Performance of NiFe-LDH via Sn Doping toward the Water Oxidation Reaction under Alkaline Condition, *Inorg. Chem*. 2022, **61**, 16895-16904.

[3] J. Ding, M. Zhang, X. Wei, W. Song, J. Wang, T. Sun, J. Zhu, M. Wang, An advanced NiFe-LDH nanoclusters arrays for high-efficient full water splitting, *J. Mater. Sci.* 2021, **56**, 19466-19475.

[4] Q. Dong, C. Shuai, Z. Mo, N. Liu, G. Liu, J. Wang, H. Pei, Q. Jia, W. Liu, X. Guo, CeO_2 nanoparticles @ NiFe-LDH nanosheet heterostructure as electrocatalysts for oxygen evolution reaction, J. Solid. State. *Chem*. 2021, **296**, 121967.

[5] Y. Liao, R. He, W. Pan, Y. Li, Y. Wang, J. Li, Y. Li, Lattice distortion induced Ce-doped NiFe-LDH for efficient oxygen evolution, *Chem. Eng. J*. 2023, **464**, 142669.

[6] L. Wang, J. Wang, X. Wang, M. Li, J. Wei, N. Hu, R. Xu, L. Yang, Constructing NiFe-LDH@$Ni_xCo_ySe_2$/NF nanosheets heterojunction for high-current-density efficient water oxidation, *Appl. Surf. Sci.* 2023, **607**, 154589.

[7] L. Xiao, W. Bao, J. Zhang, C. Yang, T. Ai, Y. Li, X. Wei, P. Jiang, L. Kou, Interfacial interaction between NiMoP and NiFe-LDH to regulate the electronic structure toward high-efficiency electrocatalytic oxygen evolution reaction, *Int. J. Hydrogen Energ*. 2022, **47**, 9230-9238.

[8] M. Yan, Y. Zeng, Y. Mou, J. Hu, W. Tang, C. Jiang, Q. Li, Y. Zhao, Interfacial electronic regulation on $NiCo_2O_4$ nanowires@NiFe-LDH nanosheets heterostructure for efficient oxygen evolution, *J. Alloy. Compd.* 2023, **931**, 9230-9238.

[9] P. Zhang, L. Chen, L. Ge, P. Song, R. Xie, B. Wang, Y. Fu, S. Jia, T. Liao, Y. Xiong, Y. A 3D rGO-supported $NiFe_2O_4$ heterostructure from sacrificial polymer-assisted exfoliation of NiFe-LDH for efficient oxygen evolution reaction, *Carbon*. 2022, **200**, 422-429.

[10] H. Zhou, H. Wang, C. Lai, Z. Guo, J. Hu, S. Ji, L. Lei, Hierarchical heterogeneous NiFe-LDH/Ni/NM nanosheets grown in situ for stably overall water splitting at large current densities, J. Electroanal. Chem. 2022, **919**, 116527.